Developmental Biology 404 (2015) 88–102

Contents lists available at ScienceDirect

Developmental Biology

journal homepage: www.elsevier.com/locate/developmentalbiology

ROBO2 restricts the nephrogenic field and regulates Wolffian duct–nephrogenic cord separation

Elanor N. Wainwright [1], Dagmar Wilhelm [2], Alexander N. Combes [3], Melissa H. Little [4], Peter Koopman *

Institute for Molecular Bioscience, The University of Queensland, Brisbane, QLD 4072, Australia

ARTICLE INFO

Article history:
Received 7 April 2015
Received in revised form
28 May 2015
Accepted 30 May 2015
Available online 23 June 2015

Keywords:
Kidney
Wolffian duct
Ureteric bud
Nephrogenic cord
Mouse

ABSTRACT

ROBO2 plays a key role in regulating ureteric bud (UB) formation in the embryo, with mutations in humans and mice leading to supernumerary kidneys. Previous studies have established that the number and position of UB outgrowths is determined by the domain of metanephric mesenchymal *Gdnf* expression, which is expanded anteriorly in *Robo2* mouse mutants. To clarify how this phenotype arises, we used high-resolution 3D imaging to reveal an increase in the number of nephrogenic cord cells, leading to extension of the metanephric mesenchyme field in *Robo2*-null mouse embryos. *Ex vivo* experiments suggested a dependence of this effect on proliferative signals from the Wolffian duct. Loss of *Robo2* resulted in a failure of the normal separation of the mesenchyme from the Wolffian duct/ureteric epithelium, suggesting that aberrant juxtaposition of these two compartments in *Robo2*-null mice exposes the mesenchyme to abnormally high levels of proliferative stimuli. Our data suggest a new model in which SLIT-ROBO signalling acts not by attenuating *Gdnf* expression or activity, but instead by limiting epithelial/mesenchymal interactions in the nascent metanephros and restricting the extent of the nephrogenic field. These insights illuminate the aetiology of multiplex kidney formation in human individuals with *ROBO2* mutations.

1. Introduction

Mammalian kidney induction is a classic developmental model of mesenchymal and epithelial tissue interactions, with reciprocal inductive and restrictive signals between these two compartments. While many of these signals have been identified (reviewed by Costantini (2012), Schedl (2007)), the issue of how these pathways spatially regulate and remodel the linear juxtaposition of mesenchyme and epithelial tissue to induce a stereotypic epithelial outgrowth is unclear.

During development, the Wolffian ducts (WDs) form around 8.0 days *post coitum* (dpc) by mesenchymal-to-epithelial transition of the dorsal part of the anterior intermediate mesoderm (Bouchard et al., 2002; Grote et al., 2006; Pedersen et al., 2005). Subsequently, the paired WDs extend in a caudal direction, terminating in the cloaca by 9.5 dpc (Bouchard et al., 2002). The remaining ventral intermediate mesoderm is termed the nephrogenic cord, which gives rise to the mesonephros and metanephros (rostral to caudal).

The final kidney, the metanephros, develops from an interaction between the posterior region of the nephrogenic cord (the metanephric mesenchyme, MM), and the WD, such that a single ureteric bud (UB) is induced from the lateral WD (Pichel et al., 1996; Sainio et al., 1997). The WD and MM then become physically separated with the intervening ureteric mesenchyme creating a barrier preventing continued signalling interactions between the two (Bohnenpoll et al., 2013; Michos et al., 2007). Subsequently, the UB undergoes extensive branching to eventually form the collecting ducts of the kidney (reviewed by Little et al. (2010)). The MM gives rise to both the cap mesenchyme (nephron progenitor cells) that undergo a balance of self-renewal and differentiation to sequentially form epithelial nephrons (Kobayashi et al., 2008; Short et al., 2014), and the stromal elements of the final kidney (Humphreys et al., 2010).

Outgrowth of a single UB from the WD is a highly regulated process (Michos et al., 2007) with glial cell-line derived neurotrophic factor, GDNF, being the central factor. Prior to UB development *Gdnf* is expressed in the nephrogenic cord with its

* Corresponding author. Fax: +61 7 3346 2101.
E-mail address: p.koopman@imb.uq.edu.au (P. Koopman).
[1] Present address: Cancer Epigenetics Laboratory, Francis Crick Institute, Lincoln's Inn Fields Laboratories, London WC2A 3PX, UK.
[2] Present address: Department of Anatomy and Developmental Biology, Monash University, Clayton, VIC 3800, Australia.
[3] Present address: Department of Anatomy & Neuroscience, University of Melbourne, Melbourne, 3010 VIC, Australia.
[4] Present address: Murdoch Children's Research Institute, Royal Children's Hospital, Parkville, VIC 3052, Australia.

http://dx.doi.org/10.1016/j.ydbio.2015.05.023
0012-1606/

receptor RET and co-receptor GFRα1 expressed along the length of the WD (Hellmich et al., 1996; Pachnis et al., 1993; Suvanto et al., 1996). As outgrowth of the UB commences at 10.5 dpc, expression of *Gdnf* is restricted to the posterior nephrogenic cord where the UB forms (Grieshammer et al., 2004). Biochemical assays have clarified the transcriptional network regulating *Gdnf* expression, showing that SIX2 and the HOX11/EYA1/PAX2 complex directly transactivate the *Gdnf* promoter (Brodbeck et al., 2004; Gong et al., 2007). Disruption of the *Gdnf* gene in mouse results in either renal agenesis from a lack of UB induction or severe renal dysgenesis (Moore et al., 1996; Pichel et al., 1996; Sanchez et al., 1996). Furthermore, ectopic expression of *Gdnf* along the WD is sufficient to induce supernumerary UBs, cementing the importance of correct temporal–spatial control *Gdnf* expression (Shakya et al., 2005).

Previous studies have also defined a role for the secreted signalling molecule SLIT2 and its transmembrane receptor ROBO2 in the early stages of kidney development. ROBO-SLIT signalling regulates cell migration in a number of tissues, including axon guidance at the central nervous system midline (Seeger et al., 1993; Rothberg et al., 1988), migration of vascular endothelial cells towards a chemoattractive gradient (Jones et al., 2009; Park et al., 2003), migration of ventral muscle precursor cells (Kramer et al., 2001), and migration of foregut mesoderm away from the dorsal body wall (Domyan et al., 2013). The common theme among these roles is a repulsive mechanism by which ROBO-expressing cells are guided away from a source of SLIT protein (Piper and Little, 2003).

Loss-of-function of *ROBO2* in human and mouse results in the formation of multiplex kidneys from supernumerary UB induction (Grieshammer et al., 2004; Lu et al., 2007). During kidney induction, *Slit2* was found to be expressed along the length of the WD, whereas *Robo2* was expressed in the MM, at highest levels anteriorly. The complementarity of *Robo2* and *Gdnf* domains of expression, and the anterior expansion of *Gdnf* expression in the nephrogenic mesenchyme in *Slit2*- and *Robo2*-null mouse embryos (Grieshammer et al., 2004), have led to the prevailing model in which SLIT/ROBO signalling suppresses *Gdnf* expression in the anterior region.

The observation that several candidate transcriptional regulators of *Gdnf* expression were unaffected in *Slit2*-null embryos (Grieshammer et al., 2004), together with the normal role of SLIT-ROBO as a repulsive cell guidance mechanism, prompted us to reinvestigate the current model of SLIT/ROBO signalling operating primarily through effects on *Gdnf*. Here, we have assessed the size, cellular content and spatial location of the nephrogenic cord in *Robo2*-null embryos using high-resolution 3D imaging. We show that the entire nephrogenic field is expanded in *Robo2*-null mice, and associated with this is inappropriate nephrogenic cord cell proliferation. In addition, the nephrogenic cord fails to separate from the WD during kidney induction. Our data indicate that the SLIT2-ROBO2 pathway primarily acts to limit the nephrogenic mesenchyme field rather than directly restricting the extent of the *Gdnf* expression domain itself, thereby redefining the role of SLIT2-ROBO2 in kidney morphogenesis. Moreover, these findings imply that signalling from the WD to the MM controls the physical separation of these compartments.

2. Materials and methods

2.1. Mouse strains

The *Robo2*-null (Lu et al., 2007), *Six2TGC* (Kobayashi et al., 2008) and *Wnt5a*-null (Yamaguchi et al., 1999) mouse lines have been described previously. Wild-type embryos for expression analysis were collected from timed matings of outbred CD1 mice. For accurate staging, we counted either the total number of somites or the number of somites posterior to the hind limb (tail somites), with 9.5 dpc corresponding to 25 somites, 10.5 dpc to 8–10 tail somites or 35 somites, and 11.5 dpc to 17–18 tail somites.

2.2. Antibodies and stains

The following primary antibodies were used in immunofluorescence; rabbit anti-SIX2 (11562-1-AP; United Bioresearch Products) used at 1:600; mouse anti-E-cadherin (610182, Becton Dickinson) used at 1:200; rabbit anti-PAX2 (71-6000, Invitrogen) used at 1:200; mouse anti-SIX2 (H00010736-M01, Abnova) used at 1:100; mouse anti-WT1 (M3561, Dako Australia) used at 1:200; rabbit anti-ROBO2 (ab64158, Abcam) used at 1:200; mouse anti-BrdU (00-0103, Invitrogen) used at 1:200; goat anti-MYC tag (ab9132, Abcam) used at 1:1000; rabbit anti-SMAD1/5 (700047, Invitrogen) used at 1:200; mouse anti-β-catenin (610154, Becton Dickinson) used at 1:100; mouse anti-CRYM (TA501483, Australian Biosearch) used at 1:50; and goat anti-mouse Integrin-Alpha8 (LS-C150210, Sapphire Bioscience) used at 1:100. The secondary antibodies used were goat anti-rabbit Alexa 594 (A11034; Invitrogen), 1:200; rabbit anti-goat-HRP (R-21459, Invitrogen), 1:2000; and goat anti-mouse Alexa 488 (A11001; Invitrogen), 1:200. Finally, 40,6-diamidino-2-phenylindole (DAPI; 2 ng/l in PBS; Molecular Probes) was used at 1:1000 dilution.

2.3. Immunofluorescence

For section immunofluorescence, 7 μm paraffin sections were processed as described previously (Polanco et al., 2010) and slides were imaged using a LSM 510 Meta; Zeiss confocal microscope. For whole mount immunofluorescence, samples were processed as described previously (Wainwright et al., 2014) and imaged using an inverted LSM 510 Meta (Zeiss) confocal microscope.

2.4. In situ hybridisation (ISH)

Probes used were *Slit2* (nt 2152-3198 of *Slit2* transcript), *Foxd1* (maprobe: 5884, GUDMAP) (Little et al., 2007), *Tbx18* (maprobe: 5257, GUDMAP) and *Wnt4* (nt 17-1099 of *Wnt4* transcript). Section ISH was performed as previously described (Wilhelm et al., 2007) with hybridisation of the probes at 60 °C. Whole mount ISH was performed as previously described (Hargrave and Koopman, 1999) with hybridisation of the probes at 65 °C. The colour reactions were performed for equal amounts of time on *Robo2*-null and wild-type embryo samples.

2.5. Ex vivo culture

HEK-C and HEK-*Slit2* cells have been described previously (De Bellard et al., 2003). HEK-C or HEK-*Slit2* cells were grown to 80% confluence in a 6-well plate and incubated for 24 h with 2 mL of culture media as detailed in (Barak et al., 2012). The supernatant of the conditioned media was then used in nephrogenic zone culture. Briefly, MM was manually dissected from 11.5 dpc kidneys after 10 min digestion with 0.25% collagenase (C5138-100MG; Sigma) in 10% foetal calf serum/PBS at 37 °C. Dissected nephrogenic zone was placed on a filter (HAWPO1300; Millipore) suspended on HEK-C or HEK-*Slit2* conditioned media supplemented with 1 μg/mL Heparin (Sigma), 400 ng/mL FGF9 (273-F9-025; Bio-Scientific), 50 ng/mL BMP7 (354-BP-010/CF; Bio-Scientific) as detailed in Barak et al. (2012) and cultured overnight at 37 °C. For kidney explant culture, urogenital tissue was grown on 6.5 mm diameter 3 μm pore Transwell filters (3415; Sigma) suspended on culture media containing Dulbecco's Modified Eagle Medium (10313-039; Invitrogen), 10% foetal calf serum, 1% Penicillin–Streptomycin (15070-063; Invitrogen), with or

without 400 ng/mL of recombinant GDNF protein (512-GF-010; Bioscientific) for 48 h at 37 °C.

2.6. Western blot

Briefly, 5 μL of cell culture supernatant was fractionated on a 10% SDS-PAGE gel and transferred onto an Immobilon-P membrane (IPVH00010; Merck). Subsequently, the membrane was blocked in 10% skim milk powder/PBS with 0.1% Tween (PBST) for 1 h at room temperature before incubation with the primary antibody diluted in blocking solution overnight at 4 °C. The membrane was washed three times in PBST before incubation with the secondary antibody diluted in blocking solution for one hour at room temperature. The membrane was then washed three times in PBST before incubation with ECL substrate Clarity (1705061; Bio-rad) for 10 min. The signal was captured by ChemiDoc MP System (Bio-rad).

2.7. Cell proliferation studies

BrdU labelling reagent (00-0103; Invitrogen) was intraperitoneally injected into pregnant mice (0.2 mL of per 20 g body weight) at 10.5 dpc and the embryos were harvested after 30 min. Embryos were fixed in 4% PFA overnight, washed in PBS, dehydrated and embedded in paraffin. Section immunofluorescence with high pH antigen retrieval was performed to denature the DNA and detect BrdU and SIX2. For BrdU quantification of the nephrogenic cord, samples were de-identified and every second 7 μm section over a 210 μm interval anterior to the prospective ureteric bud (as assessed by dilation of the WD and relative position to the hind limb) was imaged for BrdU and SIX2 staining. The number of BrdU/SIX2$^+$ cells was determined using the cell counter tool in ImageJ software and expressed as a proportion of the total number of SIX2$^+$ cells.

To assess cell proliferation in nephrogenic zone cultures after 24 h, EdU (C10085; Invitrogen) was diluted to 10 μM in the explant culture media and incubated at 37 °C for 2 h. Subsequently, the tissue was fixed for 15 min at room temperature in 4% PFA/PBS and blocked overnight in 3% bovine serum albumin (BSA)/PBS. The next day, whole mount immunofluorescence was performed as described above for SIX2, and EdU was detected as per manufacturers instructions (C10085; Invitrogen). For EdU quantification of the nephrogenic zone culture, the number of EdU/SIX2$^+$ cells was determined using the cell counter tool in ImageJ software on 3 de-identified images taken at 40 × magnification, and expressed as a proportion of the total number of SIX2$^+$ cells.

2.8. Image capture, analysis and processing

For whole mount immunofluorescence, serial Z-optical sections were captured for the depth of the sample. For whole mount urogenital ridges, samples were imaged on 10 × objective with a 0.7 × optical zoom, tiled over two different fields of view at 3.4 μm intervals. For 13.5 dpc kidneys, samples were imaged on a 10 × objective at 3.4 μm intervals. Optical sections were processed in Imaris software (Bitplane) to produce maximum-intensity projections. Three-dimensional rendering was performed with Imaris software surface tools.

For quantification of the relative number of SIX2$^+$ cells in 10.5 dpc urogenital ridges, Z-stacks were de-identified and every second Z-slice was used for the quantification by the cell counter tool in ImageJ software. For quantification of the distance between SIX2$^+$ cells and the WD, ImageJ software drawing tools were used to measure the shortest distance between SIX2$^+$ nuclei and WD nuclei on de-identified samples over the same 210 μm spatial interval used for BrdU analysis. The average relative fluorescence intensity of p-SMAD1/5 staining was measured from 20 cells per biological replicate using ImageJ and calculated as described previously (Gavet and Pines, 2010). Nuclear sphericity was measured as described previously (Coxam et al., 2014) for the 5 nephrogenic cord cells closest to the WD, over the same 210 μm spatial interval used for BrdU analysis.

2.9. Time-lapse imaging

Kidneys were explanted 24 h prior to imaging, and allowed to adhere to plastic 96 well flat clear bottom microplates (3603; Corning) with 250 μL of media (DMEM, 10% foetal calf serum, 1% penicillin–streptomycin) and incubated at 37 °C. For time-lapse imaging, kidneys were imaged using an inverted LSM 710 Meta (Zeiss) confocal microscope with 10 z-slices taken at 6.3 μm intervals, captured every 30 min on a 10 × objective. Manual cell tracking was performed for 10 cells per culture over a 13 h window using Imaris software.

2.10. Quantitative RT-PCR

Quantitative RT-PCR (qRT-PCR) using SYBR green (Invitrogen) was performed as described previously (Svingen et al., 2009), using MM samples from which the UB had been removed ($n=5$). Samples were normalised to the endogenous housekeeping gene *Gapdh*. The SYBR green primers used in this study are described in Supplemental Table S1.

3. Results

3.1. Robo2 is expressed in the nephrogenic cord and SIX2$^+$ metanephric mesenchyme

To define the primary defect from loss-of-function of *Robo2*, we first sought to clarify the cellular-localisation of ROBO2$^+$ cells during mesonephric and metanephric specification using immunofluorescence. At 26 somites (9.6 dpc) and 29 somites (9.8 dpc), ROBO2 was expressed in the nephrogenic cord (Fig. 1A). At 10.5 dpc, ROBO2 was expressed in SIX2$^+$ cells and a subset of WT1$^+$ cells (Fig. 1B), with WT1 expression marking coelomic epithelium, MM and gonadal somatic cells. ROBO2 expression was not detected in the ureteric mesenchyme (Fig. 1B). At 11.5 dpc, ROBO2 was detected in the SIX2$^+$ MM population of cells surrounding the UB, supporting previous findings that *Robo2* is a direct target gene of SIX2 (Fig. 1C) (Kanda et al., 2014).

The kidney phenotype of *Slit2*-null mice phenocopies *Robo2*-null mice (Grieshammer et al., 2004), suggesting that SLIT2 is the predominant ligand for ROBO2 in the kidney. Therefore, we next examined the expression of *Slit2* by *in situ* hybridisation (ISH). We detected *Slit2* expression in the WD (Fig. 1D–F) consistent with published data (Grieshammer et al., 2004). At 9.5 dpc, *Slit2* was detected only very weakly in the WD (Fig. 1D). At 10.5–11.5 dpc, *Slit2* expression was detected in the WD, the cranial and caudal mesonephric tubules, and in the ureteric tip of the emerging ureteric bud (Fig. 1E and F). Expression was weak in the WD around the site of UB outgrowth, and stronger in more anterior/mesonephric regions, suggesting that ROBO2–SLIT2 signalling may be stronger in regions anterior to the position of UB outgrowth (Fig. 1E and F).

3.2. The MM is expanded and fails to partition from the WD at 11.5 dpc

It was previously reported, based on whole mount ISH, that the domain of MM was not expanded in 11.25–11.5 dpc *Robo2*-null mice, even though the domain of *Gdnf* expression extended

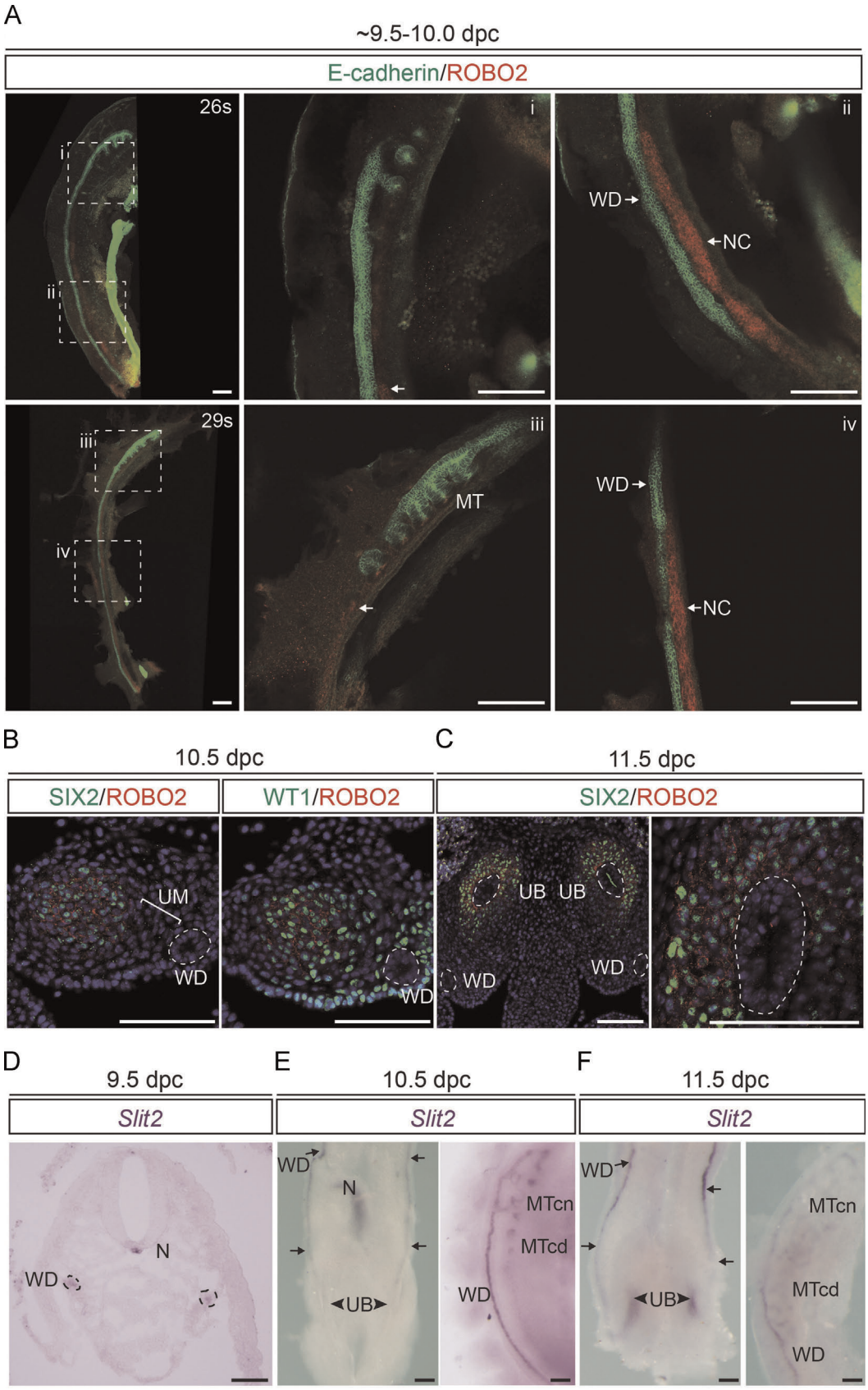

Fig. 1. ROBO2 is expressed in the nephrogenic cord and SIX2^{+} cells. (A) Whole mount immunofluorescence for ROBO2 (red), and E-cadherin (green) on dissected urogenital ridges at 26 somites (s) and 29s detected expression of ROBO2 in the nephrogenic cord adjacent to the epithelial WD. (B) Transverse section immunofluorescence for ROBO2 (red), SIX2 (green) and WT1 (green) at 10.5 dpc, indicates that ROBO2 is expressed in SIX2^{+} cells and not the ureteric mesenchyme (UM). Dotted line indicates WD. (C) Transverse section immunofluorescence for ROBO2 (red) and SIX2 (green) at 11.5 dpc indicates that ROBO2 is expressed in SIX2^{+} cells. Cell nuclei are marked by DAPI staining (blue). (D) Transverse section *in situ* hybridisation for *Slit2* at 9.5 dpc detected expression in the notochord (N) and weak expression in the WDs. (E and F) Whole mount *in situ* hybridisation for *Slit2* at 10.5 dpc (E) and 11.5 dpc (F) detected expression in the WD, UB, cranial mesonephric tubules (MTcr) and caudal mesonephric tubules (MTcd). Scale bars represent 100 μm.

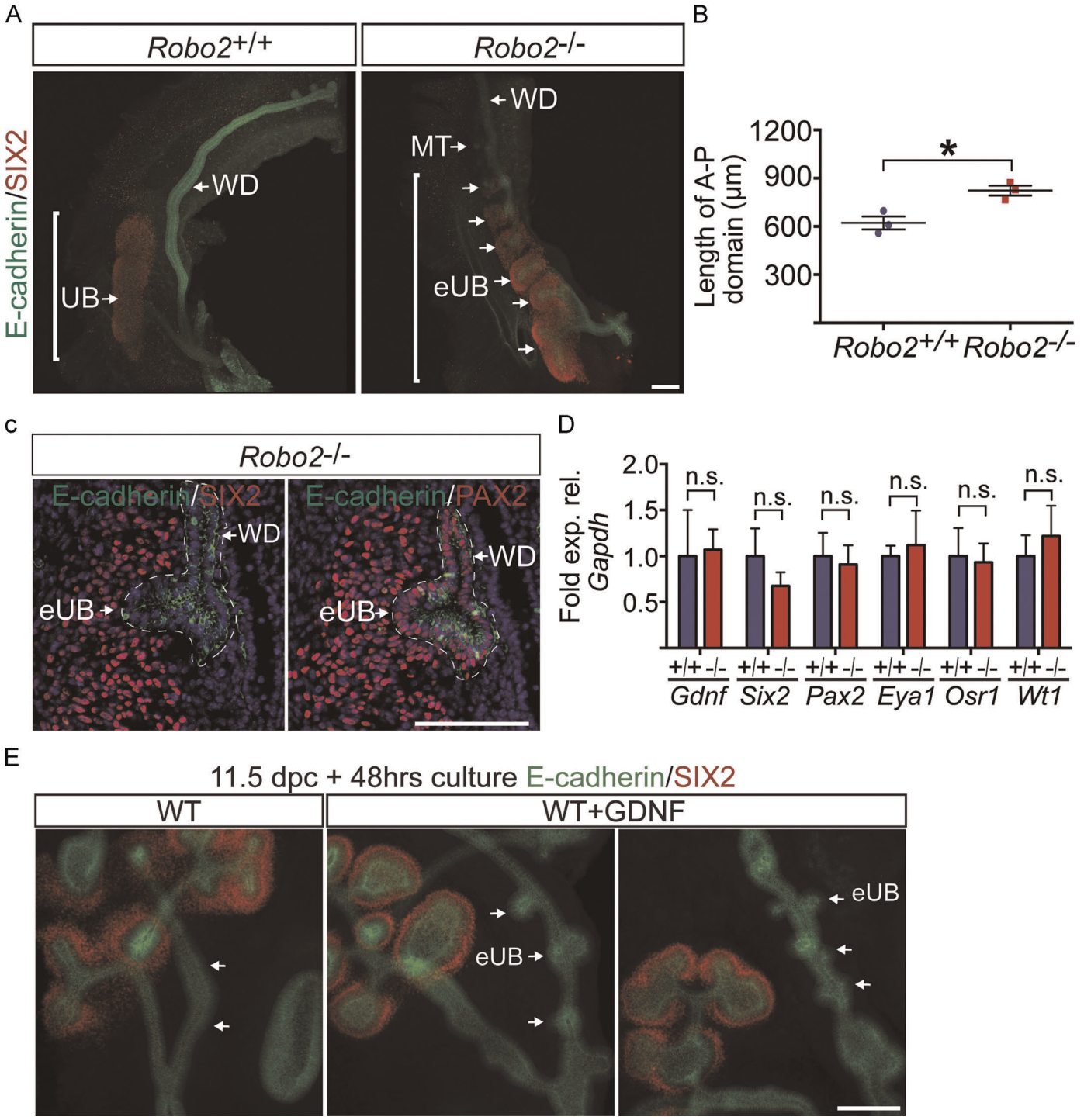

Fig. 2. The MM is lengthened upstream of *Gdnf* in *Robo2*-null embryos at 11.5 dpc (A) Whole mount immunofluorescence for SIX2 (red), marking the MM and E-cadherin (green), marking the WD, UB, ectopic UBs (eUB) and mesonephric tubules (MT), indicates that the MM was expanded and failed to separate from the WD. (B) The length of the anterior-to-posterior (A–P) domain of SIX2$^+$ cells is greater, $n=3$. $^*p=0.01642$. (C) Section immunofluorescence for PAX2 (red), marking the MM and WD and SIX2 (red) marking the MM on adjacent serial sections indicates that SIX2 and PAX2 are likely to be co-expressed in the same cells. Cell nuclei are indicated by DAPI staining (blue). Dotted line indicates WD and eUB. (D) Quantitative RT-PCR did not detect any significant changes in the expression of the MM markers, *Gdnf, Six2, Eya1, Pax2, Osr1* and *Wt1* in *Robo2*-null nephrogenic zone, relative to wild-type. Error bars represent SEM, $n=5$. (E) Whole mount immunofluorescence for SIX2 (red), marking the cap mesenchyme and E-cadherin (green), marking the WD and ureteric tree indicates that eUBs induced by exogenous GDNF are not surrounded by SIX2$^+$ mesenchyme. Arrows indicate WD with/without eUBs. Data represents three individual cultures per experiment, from two experiments performed on independent days. In all analyses, an unpaired two-tailed Student's *T*-test was used to assess statistical significance, n.s. not significant, Scale bars represent 100 μm.

anteriorly (Grieshammer et al., 2004). We first validated that *Gdnf* expression domain was indeed expanded at 11.25 dpc (Supplemental Fig. S1A). Subsequently, we re-investigated the expansion of upstream transcriptional regulators of *Gdnf* expression using high-resolution whole mount and section immunofluorescence with antibody markers for the MM (SIX2, PAX2) and WD/UB (E-cadherin, PAX2). Surprisingly, the domain of SIX2$^+$ cells was expanded in *Robo2*-null embryos compared to wild-type controls at 11.25–11.5 dpc (Fig. 2A, B, Supplemental Fig. 1B). Analysis of serial sections through the nephrogenic region at the level of the most

anterior ectopic UB indicated that SIX2 and PAX2 are likely expressed in the same cells, suggesting that both SIX2 and PAX2 cell domains are expanded (Fig. 2C).

In addition to an expanded MM domain, we examined if the levels of *Gdnf* per cell, or the expression of other regulators of the MM, were perturbed. Quantitative RT-PCR of manually dissected MM from *Robo2*-null embryos and wild-type controls at 11.5 dpc revealed that there was no significant change in the expression levels of *Gdnf*, *Six2*, *Pax2*, *Osr1*, *Eya1* or *Wt1* in the MM, suggesting that, at a cellular level, the MM transcriptional hierarchy was normal (Fig. 2D).

3.3. Ectopic UBs stimulated by exogenous GDNF do not induce a SIX2+mesenchyme

Since SIX2 is a direct transcriptional activator of *Gdnf* expression (Brodbeck et al., 2004; Gong et al., 2007), our observation that the SIX2 expression domain was expanded suggested that an increase in the MM is the underlying cause of expansion of *Gdnf* expression in *Robo2*-null embryos. However, to exclude the possibility that GDNF-induced ectopic UBs can up-regulate SIX2 expression in associated cells, 11.5 dpc urogenital ridges were cultured with 400 ng/mL of recombinant rat GDNF for 48 h. Ectopic WD budding stimulated by exogenous GDNF did not induce an associated SIX2$^+$ mesenchyme (Fig. 2E), confirming that an expansion of the SIX2$^+$ expression domain is not secondary to expansion of *Gdnf* expression (Shakya et al., 2005).

3.4. Expansion of the metanephric field perturbs the mesonephric field

With the observed anterior expansion of the metanephros in *Robo2*-null mice, we next examined the consequences that this had on the patterning of the mesonephros at 13.5 dpc (Fig. 3A). PAX2 and E-cadherin immunofluorescence of the mesonephros revealed that ectopic ureteric buds extended into the gap region of the mesonephros in *Robo2*-null embryos (Fig. 3A and B). These ectopic ureteric buds phenotypically resembled developing kidneys, displaying branching and PAX2$^+$-associated mesenchyme, supporting our earlier finding that the SIX2/PAX2 metanephric field is expanded in *Robo2*-null embryos. In addition, examination of the mesonephric tubules across the cranial-caudal regions revealed that the number of cranial tubules was unchanged, but there was a significant increase in the number of caudal mesonephric tubules in the *Robo2*-null mesonephros compared to wild-type (Fig. 3A–C).

3.5. The number of SIX2$^+$ cells is increased in Robo2-null mice

The nephrogenic cord gives rise to the caudal mesonephric tubules and the MM, suggesting a possible early expansion of this cell population in *Robo2*-null embryos compared to wild-type. To test this hypothesis, the nephrogenic cord domain was investigated at 10.5 dpc, prior to invasion of the UB/s (Fig. 3D).

First, the anterior–posterior domain of SIX2$^+$ cells was measured based on confocal images, which did not reveal any significant difference between *Robo2*-null embryos compared to wild-type, suggesting that anterior–posterior expansion of the SIX2$^+$ domain does not precede UB induction (Fig. 3E). Second, the diameter of the field of SIX2$^+$ cells had a similar diameter in *Robo2*-null embryos compared to wild-type at the most posterior end (Fig. 3F). However, there was a significantly wider diameter of the field of cells in *Robo2*-null embryos at a more anterior level correlating to the anterior metanephros/caudal mesonephros, suggesting that the compaction or number of cells was disrupted (Fig. 3G). Third, the relative number of cells was quantified, revealing an ~30% increase in the number of SIX2$^+$ cells in *Robo2*-null compared to wild-type urogenital ridges (Fig. 3H). Therefore the number of cells in the nephrogenic mesenchyme was increased, with broadening of the anterior metanephric/ caudal mesonephric region of the cord.

3.6. Increased rate of proliferation of Robo2-null MM is dependant on the WD

Since more SIX2$^+$ cells were identified at 10.5 dpc, we next examined the rate of cell proliferation in the anterior metanephros/posterior mesonephros. BrdU labelling showed that, over a 210 μm interval anterior to the presumptive position of the UB (Fig. 4A), significantly more SIX2$^+$ cells were in S-phase of the cell cycle in *Robo2*-null embryos compared to wild-type (Fig. 4B and C). Thus, the increase in the number of nephrogenic cord cells at 10.5 dpc likely resulted from an increase in proliferation.

To investigate whether active ROBO2–SLIT2 signalling has a direct effect on cell proliferation of SIX2$^+$ cells, 11.5 dpc wild-type MM was physically separated from the UB to remove the SLIT2 source and cultured in media conditioned with or without recombinant SLIT2 (Fig. 4D) (De Bellard et al., 2003). Culturing the MM for 24 h with SLIT2 did not significantly change the incorporation of EdU in SIX2$^+$ cells (Fig. 4E and F).

To control for a possible SLIT2-independent effect on proliferation, or redundancy with any unknown ROBO2 ligand/s that may have been secreted by the MM, we compared the relative rate of proliferation of *Robo2*-null, -heterozygous and wild-type MM *ex vivo*. There was no significant difference in the rate of EdU incorporation in the MM cultures between *Robo2*-null and wild-type littermates (Fig. 4G, H). Hence, these data suggest that SLIT2 signalling *via* the ROBO2 receptor is not a direct mitosis-inhibiting signal.

3.7. SIX2$^+$cells fail to separate from the WD in Robo2-null mice

The fact that increased proliferation within the SIX2$^+$ MM domain *in vivo* resulted in an expanded domain, but *ex vivo* addition of SLIT2 protein did not influence the rate of cell proliferation, suggested the possibility of a WD-derived signal driving proliferation of SIX2$^+$ cells in the absence of *Robo2*. Therefore, we re-examined the spatial relationship between the SIX2$^+$ domain and the WD. At 11.5 dpc, the SIX2$^+$ domain was not only expanded, but also localised closer to the WD in *Robo2*-null compared to wild-type embryos (Fig. 2A). While the MM exclusively associated with the tip domain of the UB in wild-type mice, the MM enveloped sections of the ureteric stalks and WD in *Robo2*-null embryos (Fig. 2A).

Since the MM failed to partition from the WD, we examined if the other mesenchymal lineages of the kidney were mis-specified or mislocalised at 11.5 dpc. Marker analysis examining PAX2 and WT1, with double-positive cells representing the MM, further confirmed a direct association of some MM cells with the WD in *Robo2*-null embryos (Fig. 5A). *Foxd1* marks the kidney stroma, with the stroma contributing to non-epithelial kidney structures, and is required to promote the differentiation of SIX2$^+$ cells (Das et al., 2013). In both *Robo2*-null and wild-type embryos, *Foxd1* localised around the periphery of the condensed mesenchyme surrounding the UBs (Fig. 5B). *Tbx18* is expressed in the ureteric mesenchyme, a domain of mesenchyme separating the MM and WD at 11.5 dpc (Bohnenpoll et al., 2013). Section ISH for *Tbx18* identified that *Tbx18*-expressing cells were localised in a more lateral position in *Robo2*-null embryos rather than localised between the developing UB tip/metanephric mesenchyme and the WD in wild-type embryos (Fig. 5C). Thus, the required kidney mesenchymal compartments are specified but the ureteric

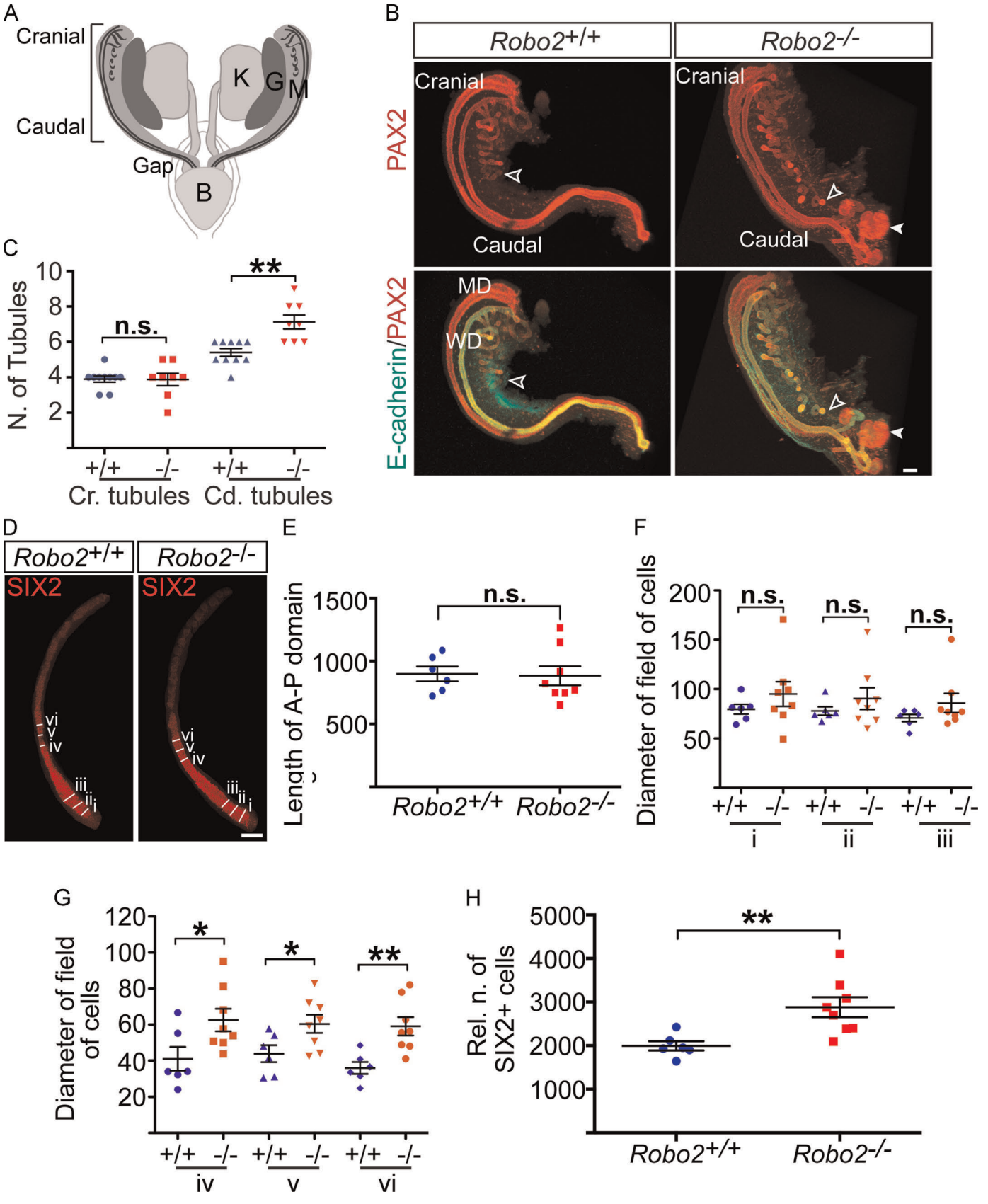
A
Cranial
Caudal
K
G
M
Gap
B
B
Robo2+/+
Robo2-/-
PAX2
Cranial
Caudal
E-cadherin/PAX2
MD
WD
C
N. of Tubules
n.s.
**
+/+ -/- +/+ -/-
Cr. tubules Cd. tubules
D
Robo2+/+
Robo2-/-
SIX2
vi
v
iv
iii
ii
i
E
Length of A-P domain
n.s.
Robo2+/+ Robo2-/-
F
Diameter of field of cells
n.s.
n.s.
n.s.
+/+ -/- +/+ -/- +/+ -/-
i ii iii
G
Diameter of field of cells
*
*
**
+/+ -/- +/+ -/- +/+ -/-
iv v vi
H
Rel. n. of SIX2+ cells
**
Robo2+/+ Robo2-/-

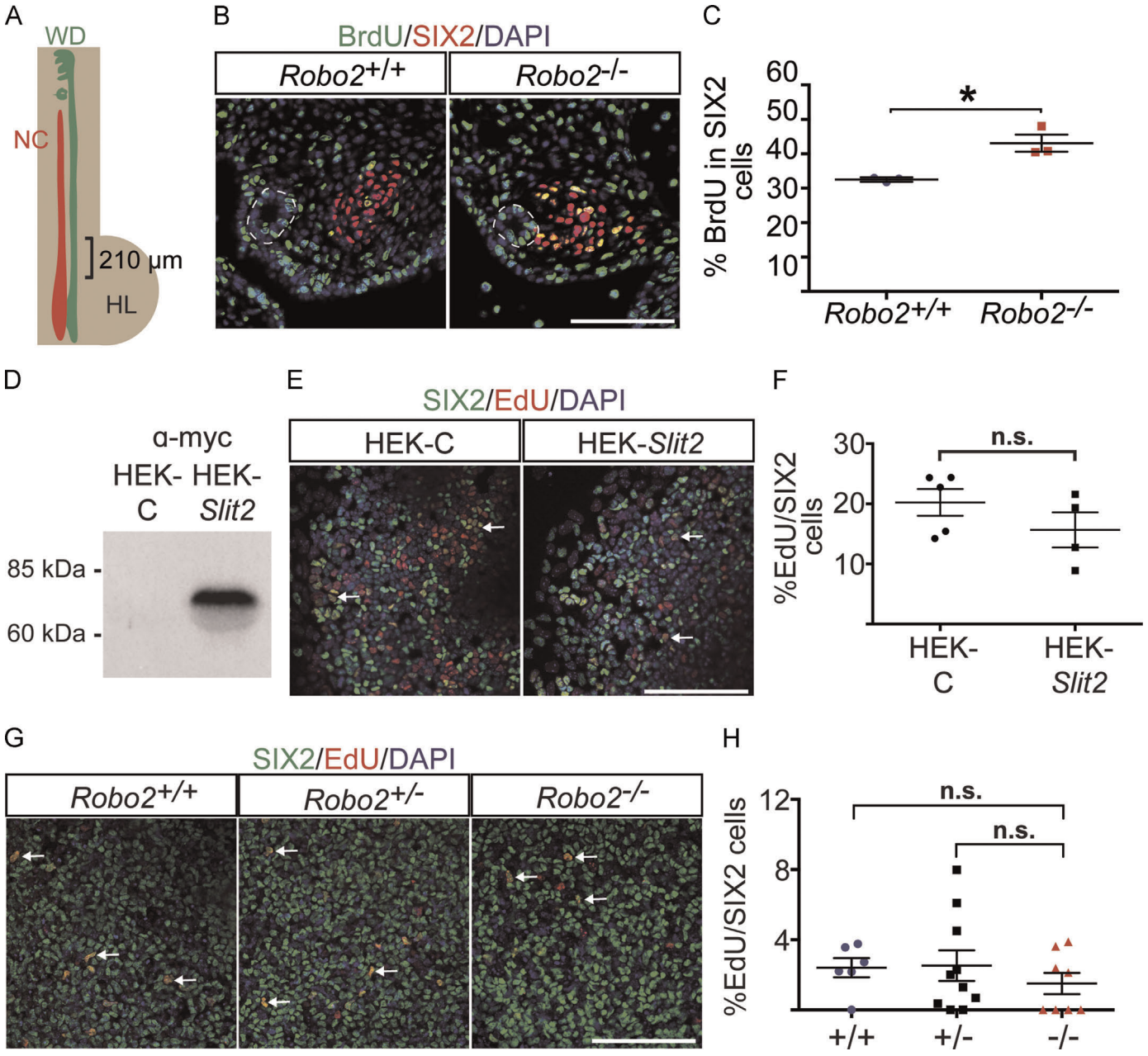

Fig. 4. ROBO2–SLIT2 signalling is not a direct mitosis-inhibiting signal *ex vivo*. (A) A schematic indicating the region of analysis for proliferation of nephrogenic cord cells relative to the hind limb (HL). (B) Transverse section immunofluorescence for SIX2 (green) and BrdU (red), suggested that more SIX2$^+$ cells were BrdU$^+$ in *Robo2*-null mice compared to wild-type at 10.5 dpc. Cell nuclei are marked by DAPI (blue). Dotted line indicates WD. (C) Quantification of the percentage of BrdU$^+$/SIX2$^+$ cells indicates that a significantly higher percentage of BrdU$^+$/SIX2$^+$ cells are present in *Robo2*-null mice, compared to wild-type. $n=3$. $^*p=0.01338$. (D) Western blot for a C-terminal MYC-tag of SLIT2 in conditioned media from human embryonic kidney (HEK) control (C) conditioned media and HEK-SLIT2 showed that that cleaved SLIT2 was secreted into the media. (E) Immunofluorescence for SIX2 (green) and EdU (red) indicates dividing cells in MM culture with or without exogenous SLIT2. Cell nuclei are marked by DAPI staining (blue). (F) Quantification of the percentage of EdU$^+$/SIX2$^+$ cells did not identify a significant difference in the rate of proliferation of SIX2 cells within the nephrogenic zone cultured with or without SLIT2. Each point represents an individual cap culture, from experiments performed on three independent days. (G) Immunofluorescence for SIX2 (green) and EdU (red) indicates dividing cells in *Robo2*-heterozygous or *Robo2*-null MM culture. Cell nuclei are marked by DAPI staining (blue). (H) Quantification of the percentage of EdU$^+$/SIX2$^+$ cells did not identify a significant difference (n.s.) in the rate of proliferation of nephrogenic zone culture between *Robo2*-heterozygous, *Robo2*-null and wild-type samples. Each point represents an individual nephrogenic zone culture, from experiments performed on four independent days. In all analyses, an unpaired two-tailed Student's *T*-test was used to assess statistical significance. Scale bars represent 100 μm.

Fig. 3. More SIX2-expressing cells are present in *Robo2*-null urogenital ridges. (A) A diagram indicating cranial, caudal and gap regions of the mesonephros (M) where presence of mesonephric tubules was examined in region indicated by bracket. Position of gonads (G), kidneys (K) and bladder (B) are also indicated. (B) Whole mount immunofluorescence for PAX2 (red), marking the WD, Müllerian duct, and mesonephric tubules and E-cadherin (green), marking the WD and mesonephric tubules, indicates that more caudal mesonephric tubules are present in *Robo2*-null embryos, compared to wild-type. Open arrowhead indicates posterior limit of mesonephric tubules and closed arrowhead indicates eUB with PAX2 condensed mesenchyme. (C) Quantification of the number (*N*) of mesonephric tubules showed that there was no change in the number of cranial (Cr) tubules, but there was a significant increase in caudal (Cd) tubules. $^{**}p=0.0010$. (D) Whole mount immunofluorescence for SIX2, indicating the levels at which the diameter of the field of SIX2$^+$ cells was measured. (E) The length (μm) of the anterior-to-posterior (A–P) domain of SIX2$^+$ cells is the same at 10.5 dpc. (F) Quantification of the diameter of the field of SIX2$^+$ cells indicates that the posterior end, i–iii or 50–150 μm vertical to the most posterior position of SIX2$^+$ cells, there is no significant difference between *Robo2*-null and wild-type, whereas at more anterior levels (G), iv–vi or 450–550 μm vertical to the most posterior position of SIX2$^+$ cells, there was a significant increase in the width of the field of cells. $n=6$–8. $^*p=0.03791$, $^*p=0.03798$, $^{**}p=0.00445$. (H) Quantification of relative number of SIX2$^+$ cells indicates a significant increase in SIX2$^+$ cells in *Robo2*-null mice relative to wild-type. $n=6$–8. $^{**}p=0.00845$. In all analyses, an unpaired two-tailed Student's t-test was used to assess statistical significance. Error bars represent SEM. Scale bars represent 100 μm.

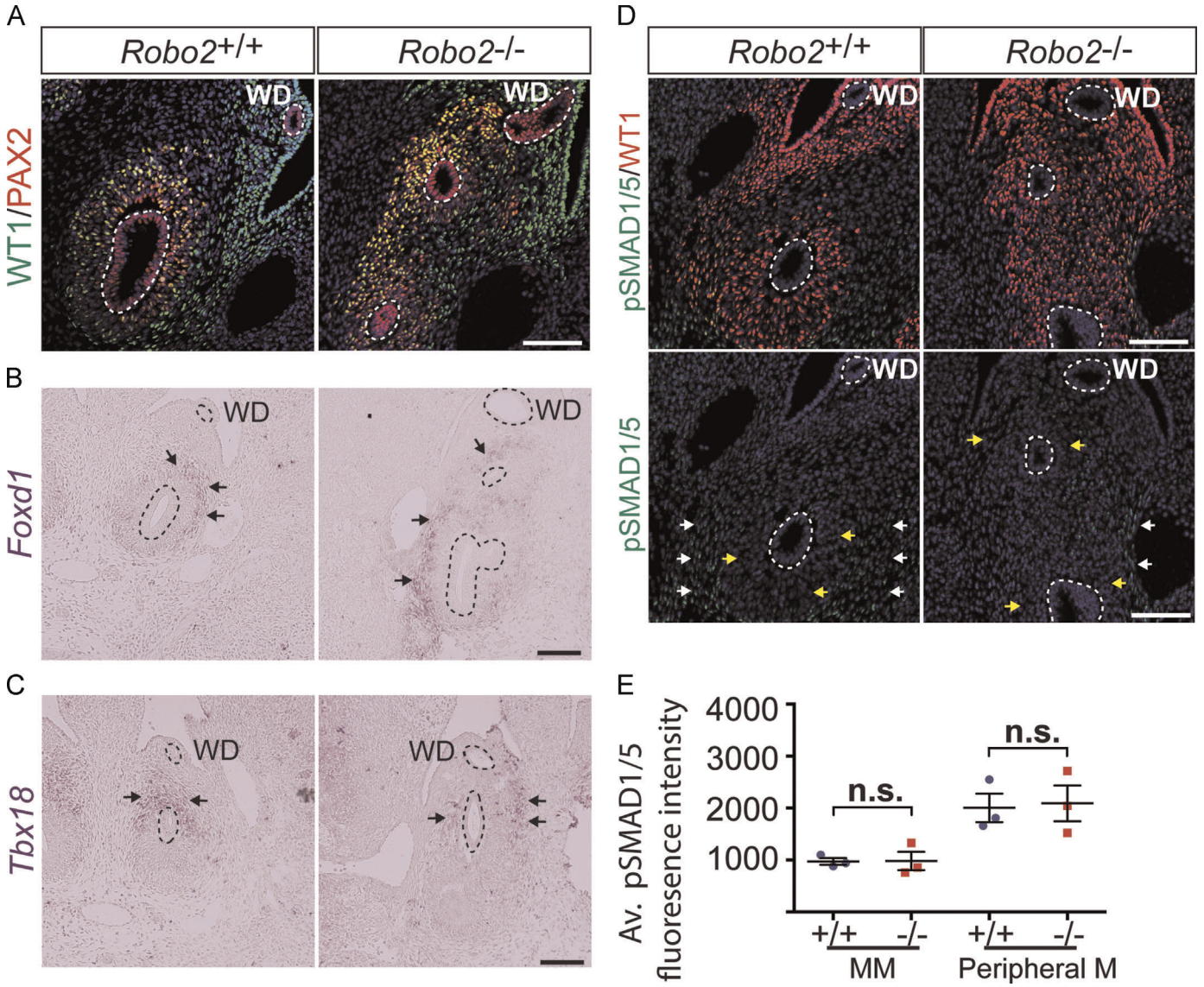

Fig. 5. The mesenchymal cell lineages of the kidney are specified but mislocalised in *Robo2*-null embryos at 11.5 dpc. (A) Transverse section immunofluorescence for PAX2 (red), marking the MM and WD, and WT1 (green), marking the MM, coelomic epithelium and ureteric mesenchyme indicates that the mesenchymal domains are mislocalised in *Robo2*-null embryos, compared to wild-type. Cell nuclei are marked by DAPI staining (blue). (B) Transverse section *in situ* hybridisation for *Foxd1* (purple), staining stromal cells, indicates that stromal cells are present in *Robo2*-null mice and are localise around UB/MM. Arrows indicate expression and dotted lines indicate WD and UB/s. (C) Transverse section *in situ* hybridisation for *Tbx18* (purple), marking ureteric mesenchyme, indicates that ureteric mesenchyme is present in *Robo2*-null mice and is more predominantly localised lateral to the UB rather than between the UB and the WD, compared to wild-type. (D) pSMAD-1/5 activation is unchanged in *Robo2*-null MM at 11.5 dpc. WT1$^+$ cells condensed around UB outgrowths (yellow arrows) have low levels of pSMAD-1/5 staining, similar to wild-type. More laterally localised non-WT1$^+$ mesenchymal cells (white arrows) show equivalent strong pSMAD-1/5 nuclear staining to those in wild-type. (E) The average pSMAD1/5 fluorescence intensity was the same between *Robo2*-null and wild-type MM and non-WT1$^+$ peripheral mesenchyme (M). An unpaired two-tailed Student's *T*-test was used to assess statistical significance, $n=3$.

mesenchyme is misplaced in *Robo2*-null embryos.

GREM1 antagonism of BMP4 signalling in the WD mesenchyme provides a permissive signal for the UB to invade the posterior MM (Michos et al., 2007). Given the observed failure of separation between the WD and MM, we examined active phospho-SMAD1/5 at 11.5 dpc and 10.5 dpc to assess whether GREM1/BMP4 signalling was perturbed. There was no difference in the levels of p-SMAD1/5 staining detected in the nuclei of non-WT1$^+$ mesenchymal cells (strong staining) and in condensed MM (weak staining) in *Robo2*-null and wild-type embryos consistent with the published expression pattern (Michos et al., 2007) (Fig. 5D, E, Supplemental Fig. S2), suggesting that changes to BMP signalling do not contribute to ectopic UB induction in *Robo2*-null embryos.

3.8. ROBO2 regulates the separation of the nephrogenic cord and WD at 10.5 dpc

Next, we examined if mislocalisation of SIX2$^+$ cells could contribute to ectopic UB induction in *Robo2*-null embryos by examining the position of the nephrogenic cord at 10.5 dpc. Strikingly, SIX2$^+$ cells were closer to the WD in *Robo2*-null compared to wild-type mice (Fig. 6A and B). This juxtaposition was also evident in whole mount immunofluorescence for SIX2 and E-cadherin (Fig. 6C). Thus, unlike the situation in wild-type embryos, SIX2$^+$ cells were in close association with the WD prior to observable UB outgrowths in *Robo2*-null embryos, consistent with a role for the WD in regulating proliferation of SIX2$^+$ cells.

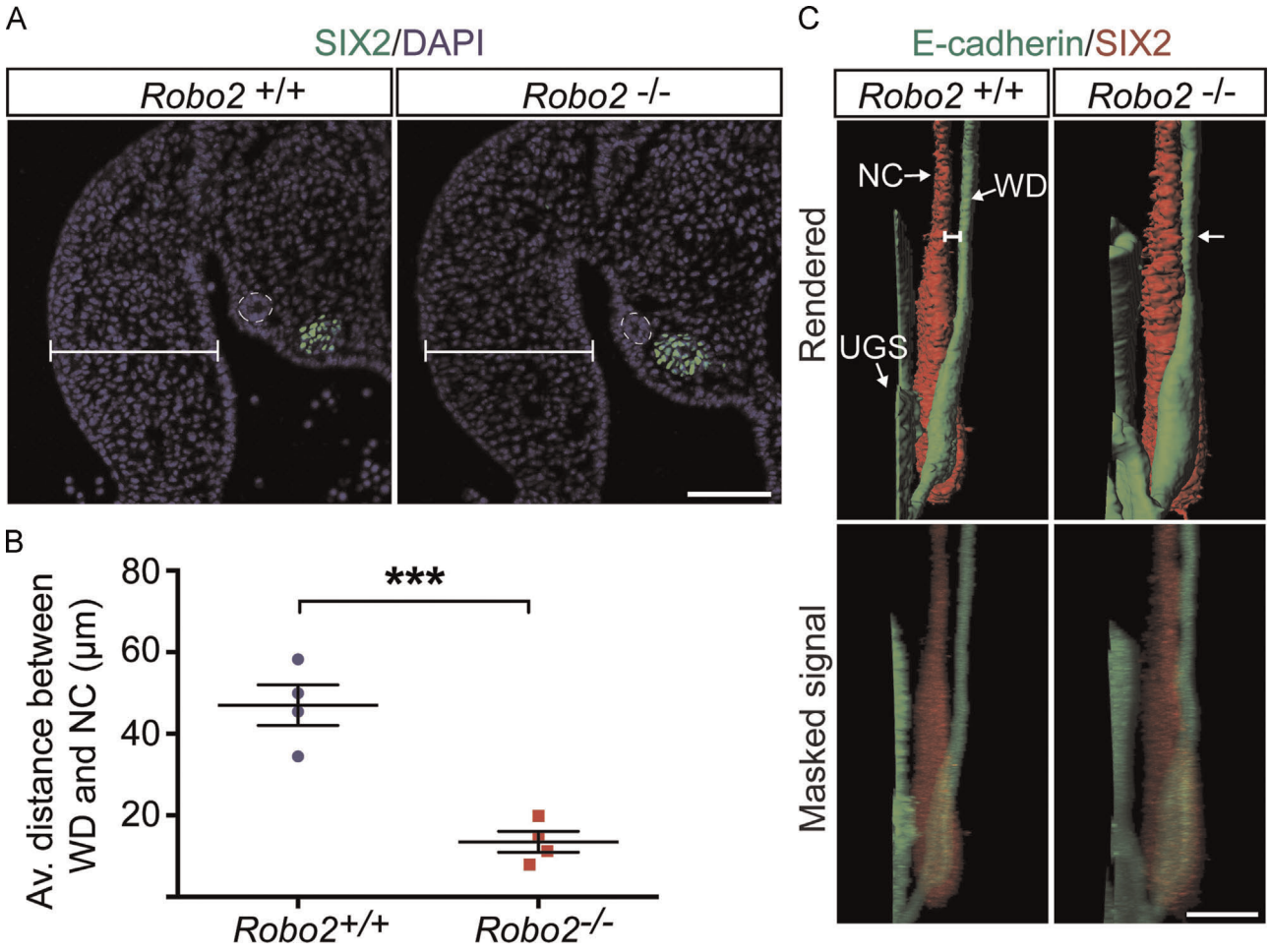

Fig. 6. SIX2$^+$ cells are mislocalised prior to UB outgrowth in *Robo2*-null embryos at 10.5 dpc. (A) Transverse section immunofluorescence for SIX2 (green) indicates that the SIX2$^+$ field of cells is localised closer to the WD in *Robo2*-null embryos compared to wild-type. Width of the hind limb is equivalent as indicated by bar. Cell nuclei are marked by DAPI staining (blue). WD is circled by dotted line. (B) Quantification of the average (Av) shortest distance between WD and SIX2 nuclei in the anterior metanephros over a 210 μm interval identified a significant decrease in the distance between the WD and SIX2 cells in *Robo2*-null mice, compared to wild-type. An unpaired two-tailed Student's *T*-test was used to assess statistical significance. $n=4$. $^{***}p=0.00095$. Error bars represent SEM. (C) A rendered view of whole mount immunofluorescence for SIX2 marking the nephrogenic cord (NC) (red) and E-cadherin (green) marking the WD and urogenital sinus (UGS) indicates that SIX2$^+$-domain is closer to the WD than wild-type. Masked fluorescent signal is also shown. Scale bars represent 100 μm.

3.9. ROBO2 regulates the localisation of SIX2$^+$ cells at multiple steps in kidney development

Mislocalisation of SIX2$^+$ cells suggested that ROBO2 might regulate cell migration. To assess this possibility, we employed a live-imaging approach, using mice that express green fluorescent protein (GFP) under the control of *Six2* regulatory region, to visualise global cell movement in *Robo2*-null kidneys compared to wild-type. We examined the movement of SIX2$^+$ cells at 13.5 dpc because the fluorescent reporter was not easily visualised by confocal microscopy before prior to 13.5 dpc without excessive laser power. During kidney morphogenesis, ROBO2 expression is maintained in SIX2$^+$ cells or the cap-mesenchyme, and SLIT2 is expressed in the ureteric tips, suggesting that the pathway is functional at this stage (Piper et al., 2000). Time-lapse confocal microscopy over a 13 h interval revealed that *Robo2*-null GFP$^+$ cells maintained similar cell movements to *Robo2*-heterozygous GFP$^+$ cells, with signs of condensation around tip domains (Fig. 7A, Supplemental Movies 1 and 2). Moreover, manual cell tracking of GFP$^+$ cells did not detect any significant difference in the speed of cell movement or the overall displacement of *Robo2*-null compared to wild-type cells (Fig. 7B–D). Thus, *loss-of-Robo2* did not affect SIX2$^+$ cell movement at the resolution of whole organ growth.

Supplementary material related to this article can be found online at http://dx.doi.org/10.1016/j.ydbio.2015.05.023.

While time-lapse imaging experiments allowed a broad view of cell movement in the context of loss-of-function of *Robo2*, it did not assess if SIX2$^+$ cells were guided to the correct location. If ROBO2 was primarily acting to regulate the localisation of SIX2$^+$ cells during kidney induction, then ROBO2 would likely have a continued role in cap-mesenchyme localisation during kidney morphogenesis. At 13.5 dpc, cap mesenchyme localises to distinct niche domains around bifurcating tips of the ureteric tree in the cortical region of the kidney. Whole mount immunofluorescence revealed that the cap mesenchyme was localised to more interior positions in direct association with the ureteric tree in *Robo2*-null compared to wild-type embryos (Fig. 7E). Where SIX2$^+$ cells were localised in the interior of the kidney, ectopic branch points in the ureteric tree were present. Since multiple ureteric trees developed directly next to each other, it is possible that this mislocalisation is due to secondary interactions between neighbouring trees. Therefore, we examined SIX2$^+$ cell localisation in another mouse model of duplex kidney, *Wnt5a*-null mice (Nishita et al., 2014; Yun et al., 2014). Despite two ureteric trees growing directly next to each other, the SIX2$^+$ cap mesenchyme was still localised in the cortical region of *Wnt5a*-null kidneys (Fig. 7E), suggesting that mislocalisation of SIX2$^+$ cells is not a hallmark of ectopic UBs,

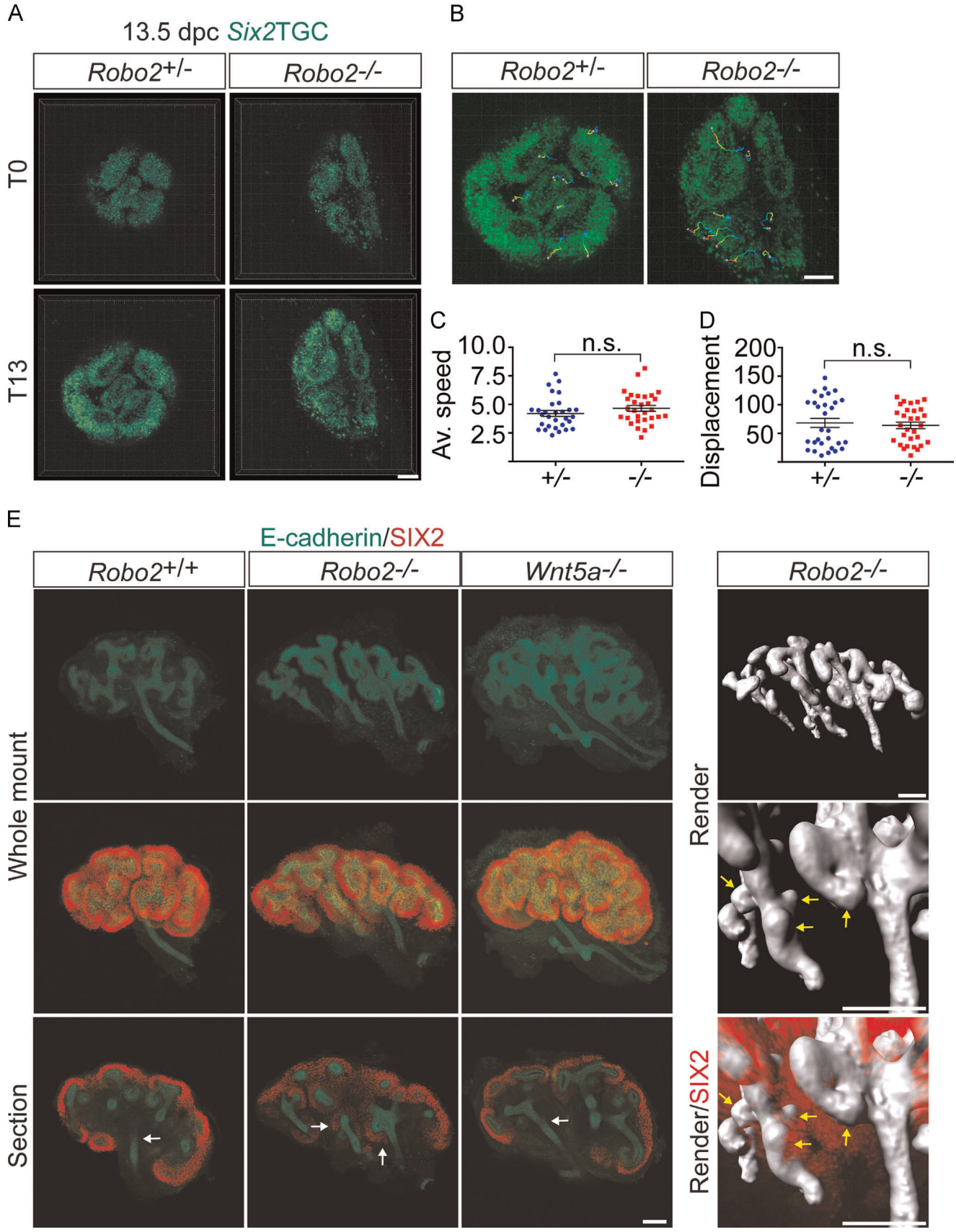

Fig. 7. Loss of *Robo2* affects localisation of cells, not global cell movement. (A) Time-lapse imaging did not detect any change in global cell movement in *Six2TGC*;*Robo2*-null and -heterozygous cultured kidneys, shown at 0 h (T0) and at 13 h (T13). (B) Tracking of cells over time-lapse imaging, where blue-to-red colouring indicates time interval. (C) The average speed of *Robo2*-null cells was the same *Robo2*-heterozygous cells, $\mu m/s \times 10^3$. (D) The average displacement of *Robo2*-null cells was the same *Robo2*-heterozygous, μm. An unpaired two-tailed Student's *T*-test was used to assess statistical significance, $n=3$. (E) Whole mount immunofluorescence for SIX2 (red), marking the cap mesenchyme and E-cadherin (green), marking the ureteric tree and nascent nephrons, indicates that $SIX2^+$ cells are localised in the interior of the ureteric tree compared to wild-type and *Wnt5a*-null mice. Scale bars represent 100 μm.

rather that it is associated with loss of ROBO2 signalling in SIX2$^+$ cells. Therefore, these data suggest that SLIT2 signalling from the epithelial kidney compartments to ROBO2-expressing SIX2$^+$ cells regulates the localisation of nephron progenitors at multiple stages of kidney development.

3.10. ROBO2 signalling regulates the polarisation of SIX2$^+$ cells

ROBO-SLIT signalling has been shown to act as a guidance cue by modulating cell adhesion in a number of cellular contexts (Domyan et al., 2013; Rhee et al., 2007). We therefore investigated expression of a key regulator of MM adhesion, Integrinα8 (Humbert et al., 2014; Linton et al., 2007), but did not detect any change in the levels of expression or localisation in *Robo2*-null MM compared to wild-type (Supplemental Fig. S3A). Activation of the ROBO receptor has also been demonstrated to impinge on β-catenin signalling (Macias et al., 2011; Rhee et al., 2007), but we did not detect any change in the levels of expression or localisation of β-catenin (Supplemental Fig. S3B), and the canonical target gene *Wnt4* (Park et al., 2007) was also unaffected in the forming renal vesicles of *Robo2*-null kidneys (Supplemental Fig. S3C). Furthermore, quantitative RT-PCR for the direct WNT target gene *Axin2* did not reveal any significant difference between *Robo2*-null and wild-type MM at 11.5 dpc (Supplemental Fig. S3D). Hence, SIX2$^+$ cells are mislocalised in *Robo2*-null embryos compared to wild-type without detriment to the expression or signalling of known adhesion molecules in the MM.

Finally, we examined how ROBO2 might regulate cell localisation by assessing the polarisation of *Robo2*-null compared to wild-type nephrogenic cord cells closest to the WD. We first assessed cell polarity by examining the orientation of the primary cilium in nephrogenic cord cells closest to the WD relative to the position of the WD. However, in both *Robo2*-null and wild-type cells ($n=3$), the angle of orientation of the primary cilium was random, suggesting that this assay does not act as a marker of cell polarisation in nephrogenic cord cells (data not shown). In addition, nuclear sphericity can be used as a proxy for directed cell migration or cell polarisation, such that cells that are migrating have more elliptical nuclei and cells that are not migrating correctly have more rounded nuclei (Coxam et al., 2014). Examination of nuclear sphericity of SIX2$^+$ cells closest to the WD revealed that *Robo2*-null cells were more rounded than wild-type cells, suggesting that SLIT2-ROBO2 signalling may regulate cell localisation by directed cell migration of nephrogenic cord cells (Fig. 8A and B).

4. Discussion

In this study we provide new mechanistic insight into the early steps of kidney development and the role of ROBO2/SLIT2 signalling in directing UB outgrowth. We show that extension of the *Gdnf* expression domain in *Robo2*-null mice is due to a lengthening of the MM domain. However, this is not the primary phenotype from loss-of-function of *Robo2*. Prior to UB induction, the nephrogenic cord itself is expanded due to an increase in the proliferation rate of *Robo2*-null nephrogenic cord cells relative to wild-type. Moreover, *ex vivo* experiments suggested that this effect on proliferation is dependant on signals from the WD and not ROBO2–SLIT2 signalling. Finally, the nephrogenic cord fails to correctly separate from the WD during kidney induction, possibly due to changes to directed cell migration. Overall we conclude that SLIT2-ROBO2 prevents inappropriate expansion of the nephrogenic mesenchyme and guides the position of the nephrogenic cord with respect to the WD, to restrict UB induction.

Based on these findings, we propose a new model for the mechanism by which SLIT/ROBO signalling restricts the number of ureteric buds that arise during kidney morphogenesis (Fig. 9A–C). Our data suggest that *loss of Robo2* primarily results in the failure of separation of the nephrogenic cord from the WD, resulting in exposure of the nephrogenic cord to proliferation signals from which it would normally be shielded by the ureteric mesenchyme (Fig. 9B). As a consequence, the number of cells in the nephrogenic cord increases, resulting in expansion of the *Gdnf* domain. The increase in the *Gdnf* domain, together with the direct association between the MM field and WD, drives ectopic UB induction (Fig. 9C). Hence, it is the balance between ROBO2-mediated separation of the nephrogenic cord from the WD and GDNF-mediated induction of WD cell proliferation and outgrowth that defines normal morphogenesis (Fig. 9A).

In regards to the movement of ureteric epithelial cells, GDNF induces chemoattractive migration of enteric neurons and a kidney epithelial cell line *in vitro* (Tang et al., 1998; Young et al., 2001). Once UB outgrowth commences, GDNF-RET is a chemotaxic/proliferative signal that drives UB outgrowth and subsequent branching morphogenesis (Chi et al., 2009; Sainio et al., 1997). At the most posterior end of the nephrogenic cord at 10.5 dpc there are more SIX2$^+$ cells compared to more anterior regions, suggesting that there is a higher concentration of GDNF in this region. On the other hand, we observed stronger staining for *Slit2* in the WD anterior to the site of UB induction, suggesting that the concentration of SLIT2 may be stronger in more anterior metanephric/

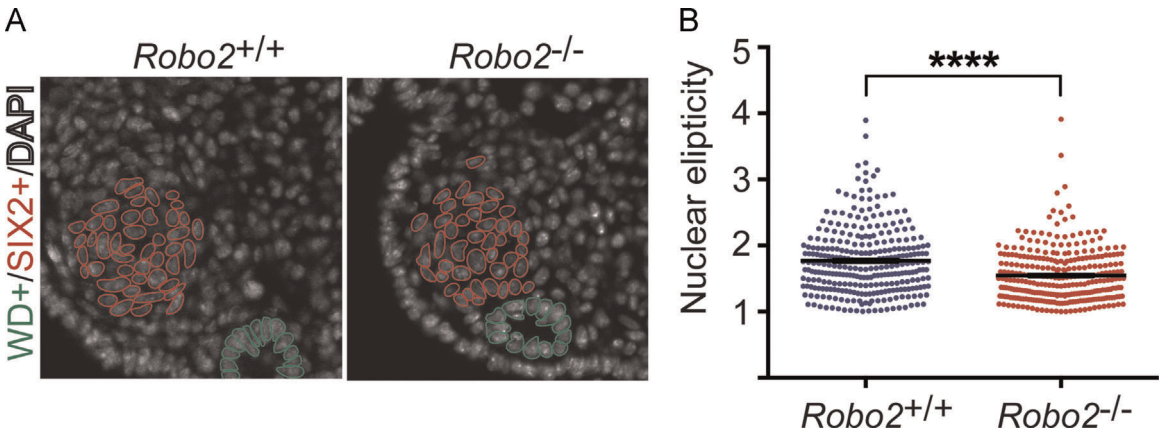

Fig. 8. *Robo2*-null nephrogenic cord cell nuclei closest to the WD are more rounded compared to wild-type. (A) Outlining the nuclei of the nephrogenic cord (red) and WD (green) indicates that the nephrogenic cord nuclei closest to the WD are more spherical, compared to wild-type. Nuclei are indicated by DAPI. (B) Measuring nuclear sphericity (the ratio between the longest length and perpendicular length of the nuclei) of the 5 nephrogenic cord cells closest to the WD per section indicates that *Robo2*-null cells are more rounded. An unpaired two-tailed Student's *T*-test was used to assess statistical significance, $n=3$, $^{****}p = 4.32867 \times 10^{-9}$.

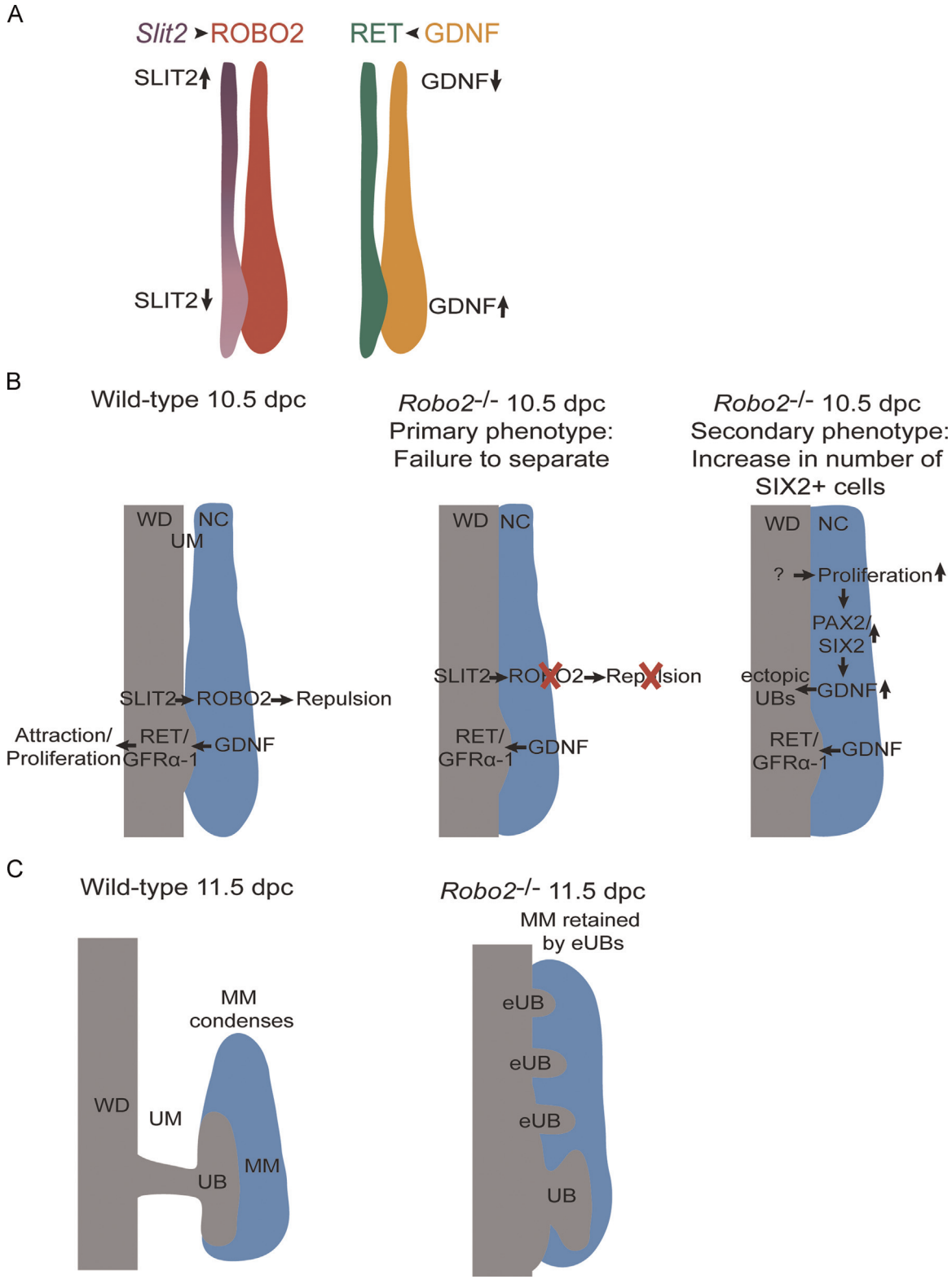

Fig. 9. A model for ROBO2 signalling in ureteric bud induction. See Section 4 for details.

caudal mesonephric regions. Perhaps UB invasion is regulated by a balance between two opposing forces: SLIT2-ROBO2 signalling guiding the MM away from the WD and GDNF-RET signalling attracting the UB towards the MM (Fig. 9A). Moreover, the strict association of the MM with ureteric tip/s during UB outgrowth, and later during branching morphogenesis, suggests that attractive and/or repulsive cues guide the position and movement of $SIX2^+$ cells.

Our finding that ROBO2-expressing $SIX2^+$ cells are mislocalised too close to the SLIT2-expressing WD suggests that *Robo2* is required for the repulsion of nephron progenitors away from the WD. On the other hand, an alternative hypothesis for the mechanism underlying the mislocalisation of $SIX2^+$ cells in *Robo2*-null mice is that mislocalisation of the mesenchyme may be a

consequence of inappropriate expansion. Indeed, experimentally confirming the repulsive cue model was problematic as micro-dissected MM tissue is difficult to culture and was not amenable to standard assays such as transwell migration assays (Domyan et al., 2013) (data not shown). However, we consider it unlikely that SLIT2-ROBO2 signalling negatively regulates SIX2 expression since when we treated SIX2$^+$ cells with or without exogenous SLIT2 *ex vivo* (Fig. 4C and D) we did not observe any changes in SIX2 expression. Moreover, exogenous treatment of kidney explants with SLIT2 did not result in any defects in nephron differentiation or maturation of nephrogenic mesenchyme (Piper M 2002), a likely consequence if SLIT2-ROBO2 signalling were a negative regulator of SIX2.

Given the consistent picture of ROBO/SLIT signalling providing repulsive cues in other organ systems (Domyan et al., 2013; Fan et al., 2003; Lundstrom et al., 2004; Park et al., 2003), we consider that ROBO2 acting as a guidance cue in the metanephros as the strongest interpretation. Our data suggest that the primary defect in *Robo2*-null mice is the result of mislocalisation since: (1) the primary signalling defect is in SIX2$^+$ cells; (2) SIX2$^+$ cells are mislocalised too close to the SLIT2 source prior to UB invasion; (3) other mesenchymal lineages of the kidney—the ureteric mesenchyme and stroma—are still specified; (4) the increase in proliferation of SIX2$^+$ cells is likely secondary to the presence of the WD and; (5) SIX2$^+$ cells are mislocalised at multiple stages of development.

The intervening mesenchyme between the WD and MM is important for the differentiation of smooth muscle cells of the ureter (Airik et al., 2006) and to create a permissive domain for UB outgrowth *via* GREM1/BMP4 antagonism (Michos et al., 2007). What draws the ureteric and WD mesenchyme between the WD and nephrogenic cord, and whether the opposing movement of the nephrogenic cord represents active migration or if the cells are simply being pushed away, is unclear. Our data suggest that the SIX2$^+$ cell lineage needs to separate from the WD for the ureteric mesenchyme to wedge between the WD and nephrogenic cord (Fig. 9B and C).

In conclusion, our data shed light on the underlying cellular events leading to multiplex kidney formation associated with loss-of-function of *Robo2* in mouse and human. While the transcriptional network active during metanephric induction and survival has been well characterised, the cellular dynamics of cells within the SIX2 population and the surrounding mesenchymal lineages of the kidney remains unclear. Further investigation of the cellular behaviour of SIX2$^+$ cells will help to refine our view of kidney morphogenesis and elucidate novel events that may be perturbed in disorders of kidney development and function such as congenital anomalies of the kidney and urinary tract (CAKUT).

Acknowledgements

We thank William Andrews and Linda Richards for *Robo2*-null mice and *HEK-C*|*HEK-Slit2* cells, Helen Cooper for providing *Wnt5a*-null mice, and Brian Key for supplying ROBO2 antibody. ML and PK are both Senior Principal Research Fellows of the NHMRC, DW is a Future Fellow of the ARC, and AC is a DECRA Fellow of the ARC. Confocal microscopy was performed at the Australian Cancer Research Foundation Dynamic Imaging Centre for Cancer Biology.

Appendix A. Supplementary Information

Supplementary data associated with this article can be found in the online version at http://dx.doi.org/10.1016/j.ydbio.2015.05.023.

References

Airik, R., Bussen, M., Singh, M.K., Petry, M., Kispert, A., 2006. Tbx18 regulates the development of the ureteral mesenchyme. J. Clin. Investig. 116, 663–674.
Barak, H., Huh, S.H., Chen, S., Jeanpierre, C., Martinovic, J., Parisot, M., Bole-Feysot, C., Nitschke, P., Salomon, R., Antignac, C., Ornitz, D.M., Kopan, R., 2012. FGF9 and FGF20 maintain the stemness of nephron progenitors in mice and man. Dev. Cell 22, 1191–1207.
Bohnenpoll, T., Bettenhausen, E., Weiss, A.C., Foik, A.B., Trowe, M.O., Blank, P., Airik, R., Kispert, A., 2013. Tbx18 expression demarcates multipotent precursor populations in the developing urogenital system but is exclusively required within the ureteric mesenchymal lineage to suppress a renal stromal fate. Dev. Biol. 380, 25–36.
Bouchard, M., Souabni, A., Mandler, M., Neubuser, A., Busslinger, M., 2002. Nephric lineage specification by Pax2 and Pax8. Genes Dev. 16, 2958–2970.
Brodbeck, S., Besenbeck, B., Englert, C., 2004. The transcription factor Six2 activates expression of the Gdnf gene as well as its own promoter. Mech. Dev. 121, 1211–1222.
Chi, X., Michos, O., Shakya, R., Riccio, P., Enomoto, H., Licht, J.D., Asai, N., Takahashi, M., Ohgami, N., Kato, M., Mendelsohn, C., Costantini, F., 2009. Ret-dependent cell rearrangements in the Wolffian duct epithelium initiate ureteric bud morphogenesis. Dev. Cell 17, 199–209.
Costantini, F., 2012. Genetic controls and cellular behaviors in branching morphogenesis of the renal collecting system. Wiley Interdiscip. Rev. Dev. Biol. 1, 693–713.
Coxam, B., Sabine, A., Bower, N.I., Smith, K.A., Pichol-Thievend, C., Skoczylas, R., Astin, J.W., Frampton, E., Jaquet, M., Crosier, P.S., Parton, R.G., Harvey, N.L., Petrova, T.V., Schulte-Merker, S., Francois, M., Hogan, B.M., 2014. Pkd1 regulates lymphatic vascular morphogenesis during development. Cell Rep. 7, 623–633.
Das, A., Tanigawa, S., Karner, C.M., Xin, M., Lum, L., Chen, C., Olson, E.N., Perantoni, A.O., Carroll, T.J., 2013. Stromal-epithelial crosstalk regulates kidney progenitor cell differentiation. Nat. Cell Biol. 15, 1035–1044.
De Bellard, M.E., Rao, Y., Bronner-Fraser, M., 2003. Dual function of Slit2 in repulsion and enhanced migration of trunk, but not vagal, neural crest cells. J. Cell Biol. 162, 269–279.
Domyan, E.T., Branchfield, K., Gibson, D.A., Naiche, L.A., Lewandoski, M., Tessier-Lavigne, M., Ma, L., Sun, X., 2013. Roundabout receptors are critical for foregut separation from the body wall. Dev. Cell 24, 52–63.
Fan, X., Labrador, J.P., Hing, H., Bashaw, G.J., 2003. Slit stimulation recruits Dock and Pak to the roundabout receptor and increases Rac activity to regulate axon repulsion at the CNS midline. Neuron 40, 113–127.
Gavet, O., Pines, J., 2010. Progressive activation of CyclinB1-Cdk1 coordinates entry to mitosis. Dev. Cell 18, 533–543.
Gong, K.Q., Yallowitz, A.R., Sun, H., Dressler, G.R., Wellik, D.M., 2007. A Hox–Eya–Pax complex regulates early kidney developmental gene expression. Mol. Cell. Biol. 27, 7661–7668.
Grieshammer, U., Le, M., Plump, A.S., Wang, F., Tessier-Lavigne, M., Martin, G.R., 2004. SLIT2-mediated ROBO2 signaling restricts kidney induction to a single site. Dev. Cell 6, 709–717.
Grote, D., Souabni, A., Busslinger, M., Bouchard, M., 2006. Pax 2/8-regulated Gata 3 expression is necessary for morphogenesis and guidance of the nephric duct in the developing kidney. Development 133, 53–61.
Hargrave, M., Koopman, P., 1999. *In situ* hybridization of whole mount embryos. In: Darby, I. (Ed.), In situ Hybridization Protocols, 2nd ed. Humana Press, Totowa, pp. 279–289.
Hellmich, H.L., Kos, L., Cho, E.S., Mahon, K.A., Zimmer, A., 1996. Embryonic expression of glial cell-line derived neurotrophic factor (GDNF) suggests multiple developmental roles in neural differentiation and epithelial–mesenchymal interactions. Mech. Dev. 54, 95–105.
Humbert, C., Silbermann, F., Morar, B., Parisot, M., Zarhrate, M., Masson, C., Tores, F., Blanchet, P., Perez, M.J., Petrov, Y., Khau Van Kien, P., Roume, J., Leroy, B., Gribouval, O., Kalaydjieva, L., Heidet, L., Salomon, R., Antignac, C., Benmerah, A., Saunier, S., Jeanpierre, C., 2014. Integrin alpha 8 recessive mutations are responsible for bilateral renal agenesis in humans. Am. J. Hum. Genet. 94, 288–294.
Humphreys, B.D., Lin, S.L., Kobayashi, A., Hudson, T.E., Nowlin, B.T., Bonventre, J.V., Valerius, M.T., McMahon, A.P., Duffield, J.S., 2010. Fate tracing reveals the pericyte and not epithelial origin of myofibroblasts in kidney fibrosis. Am. J. Pathol. 176, 85–97.
Jones, C.A., Nishiya, N., London, N.R., Zhu, W., Sorensen, L.K., Chan, A.C., Lim, C.J., Chen, H., Zhang, Q., Schultz, P.G., Hayallah, A.M., Thomas, K.R., Famulok, M., Zhang, K., Ginsberg, M.H., Li, D.Y., 2009. Slit2-Robo4 signalling promotes vascular stability by blocking Arf6 activity. Nat. Cell Biol. 11, 1325–1331.
Kanda, S., Tanigawa, S., Ohmori, T., Taguchi, A., Kudo, K., Suzuki, Y., Sato, Y., Hino, S., Sander, M., Perantoni, A.O., Sugano, S., Nakao, M., Nishinakamura, R., 2014. Sall1 maintains nephron progenitors and nascent nephrons by acting as both an activator and a repressor. J. Am. Soc. Nephrol. 25, 2584–2595.
Kobayashi, A., Valerius, M.T., Mugford, J.W., Carroll, T.J., Self, M., Oliver, G., McMahon, A.P., 2008. Six2 defines and regulates a multipotent self-renewing nephron progenitor population throughout mammalian kidney development. Cell Stem Cell 3, 169–181.
Kramer, S.G., Kidd, T., Simpson, J.H., Goodman, C.S., 2001. Switching repulsion to attraction: changing responses to slit during transition in mesoderm migration. Science 292, 737–740.
Linton, J.M., Martin, G.R., Reichardt, L.F., 2007. The ECM protein nephronectin

promotes kidney development via integrin alpha8beta1-mediated stimulation of Gdnf expression. Development 134, 2501–2509.
Little, M., Georgas, K., Pennisi, D., Wilkinson, L., 2010. Kidney development: two tales of tubulogenesis. Curr. Top. Dev. Biol. 90, 193–229.
Little, M.H., Brennan, J., Georgas, K., Davies, J.A., Davidson, D.R., Baldock, R.A., Beverdam, A., Bertram, J.F., Capel, B., Chiu, H.S., Clements, D., Cullen-McEwen, L., Fleming, J., Gilbert, T., Herzlinger, D., Houghton, D., Kaufman, M.H., Kleymenova, E., Koopman, P.A., Lewis, A.G., McMahon, A.P., Mendelsohn, C.L., Mitchell, E.K., Rumballe, B.A., Sweeney, D.E., Valerius, M.T., Yamada, G., Yang, Y., Yu, J., 2007. A high-resolution anatomical ontology of the developing murine genitourinary tract. Gene Expr. Patterns 7, 680–699.
Lu, W., van Eerde, A.M., Fan, X., Quintero-Rivera, F., Kulkarni, S., Ferguson, H., Kim, H.G., Fan, Y., Xi, Q., Li, Q.G., Sanlaville, D., Andrews, W., Sundaresan, V., Bi, W., Yan, J., Giltay, J.C., Wijmenga, C., de Jong, T.P., Feather, S.A., Woolf, A.S., Rao, Y., Lupski, J.R., Eccles, M.R., Quade, B.J., Gusella, J.F., Morton, C.C., Maas, R.L., 2007. Disruption of ROBO2 is associated with urinary tract anomalies and confers risk of vesicoureteral reflux. Am. J. Hum. Genet. 80, 616–632.
Lundstrom, A., Gallio, M., Englund, C., Steneberg, P., Hemphala, J., Aspenstrom, P., Keleman, K., Falileeva, L., Dickson, B.J., Samakovlis, C., 2004. Vilse, a conserved Rac/Cdc42 GAP mediating Robo repulsion in tracheal cells and axons. Genes Dev. 18, 2161–2171.
Macias, H., Moran, A., Samara, Y., Moreno, M., Compton, J.E., Harburg, G., Strickland, P., Hinck, L., 2011. SLIT/ROBO1 signaling suppresses mammary branching morphogenesis by limiting basal cell number. Dev. Cell 20, 827–840.
Michos, O., Goncalves, A., Lopez-Rios, J., Tiecke, E., Naillat, F., Beier, K., Galli, A., Vainio, S., Zeller, R., 2007. Reduction of BMP4 activity by gremlin 1 enables ureteric bud outgrowth and GDNF/WNT11 feedback signalling during kidney branching morphogenesis. Development 134, 2397–2405.
Moore, M.W., Klein, R.D., Farinas, I., Sauer, H., Armanini, M., Phillips, H., Reichardt, L. F., Ryan, A.M., Carver-Moore, K., Rosenthal, A., 1996. Renal and neuronal abnormalities in mice lacking GDNF. Nature 382, 76–79.
Nishita, M., Qiao, S., Miyamoto, M., Okinaka, Y., Yamada, M., Hashimoto, R., Iijima, K., Otani, H., Hartmann, C., Nishinakamura, R., Minami, Y., 2014. Role of Wnt5a-Ror2 signaling in morphogenesis of the metanephric mesenchyme during ureteric budding. Mol. Cell. Biol.
Pachnis, V., Mankoo, B., Costantini, F., 1993. Expression of the c-ret proto-oncogene during mouse embryogenesis. Development 119, 1005–1017.
Park, J.S., Valerius, M.T., McMahon, A.P., 2007. Wnt/beta-catenin signaling regulates nephron induction during mouse kidney development. Development 134, 2533–2539.
Park, K.W., Morrison, C.M., Sorensen, L.K., Jones, C.A., Rao, Y., Chien, C.B., Wu, J.Y., Urness, L.D., Li, D.Y., 2003. Robo4 is a vascular-specific receptor that inhibits endothelial migration. Dev. Biol. 261, 251–267.
Pedersen, A., Skjong, C., Shawlot, W., 2005. Lim 1 is required for nephric duct extension and ureteric bud morphogenesis. Dev. Biol. 288, 571–581.
Pichel, J.G., Shen, L., Sheng, H.Z., Granholm, A.C., Drago, J., Grinberg, A., Lee, E.J., Huang, S.P., Saarma, M., Hoffer, B.J., Sariola, H., Westphal, H., 1996. GDNF is required for kidney development and enteric innervation. Cold Spring Harb. Symp. Quant. Biol. 61, 445–457.
Piper, M., Georgas, K., Yamada, T., Little, M., 2000. Expression of the vertebrate Slit gene family and their putative receptors, the Robo genes, in the developing murine kidney. Mech. Dev. 94, 213–217.
Piper, M., Little, M., 2003. Movement through Slits: cellular migration via the Slit family. Bioessays 25, 32–38.
Polanco, J.C., Wilhelm, D., Davidson, T.L., Knight, D., Koopman, P., 2010. Sox10 gain-of-function causes XX sex reversal in mice: implications for human 22q-linked disorders of sex development. Hum. Mol. Genet. 19, 506–516.
Rhee, J., Buchan, T., Zukerberg, L., Lilien, J., Balsamo, J., 2007. Cables links Robo-bound Abl kinase to N-cadherin-bound beta-catenin to mediate Slit-induced modulation of adhesion and transcription. Nat. Cell Biol. 9, 883–892.
Rothberg, J.M., Hartley, D.A., Walther, Z., Artavanis-Tsakonas, S., 1988. slit: an EGF-homologous locus of *D. melanogaster* involved in the development of the embryonic central nervous system. Cell 55, 1047–1059.
Sainio, K., Suvanto, P., Davies, J., Wartiovaara, J., Wartiovaara, K., Saarma, M., Arumae, U., Meng, X., Lindahl, M., Pachnis, V., Sariola, H., 1997. Glial-cell-line-derived neurotrophic factor is required for bud initiation from ureteric epithelium. Development 124, 4077–4087.
Sanchez, M.P., Silos-Santiago, I., Frisen, J., He, B., Lira, S.A., Barbacid, M., 1996. Renal agenesis and the absence of enteric neurons in mice lacking GDNF. Nature 382, 70–73.
Schedl, A., 2007. Renal abnormalities and their developmental origin. Nat. Rev. Genet. 8, 791–802.
Seeger, M., Tear, G., Ferres-Marco, D., Goodman, C.S., 1993. Mutations affecting growth cone guidance in Drosophila: genes necessary for guidance toward or away from the midline. Neuron 10, 409–426.
Shakya, R., Jho, E.H., Kotka, P., Wu, Z., Kholodilov, N., Burke, R., D'Agati, V., Costantini, F., 2005. The role of GDNF in patterning the excretory system. Dev. Biol. 283, 70–84.
Short, K.M., Combes, A.N., Lefevre, J., Ju, A.L., Georgas, K.M., Lamberton, T., Cairncross, O., Rumballe, B.A., McMahon, A.P., Hamilton, N.A., Smyth, I.M., Little, M.H., 2014. Global quantification of tissue dynamics in the developing mouse kidney. Dev. Cell 29, 188–202.
Suvanto, P., Hiltunen, J.O., Arumae, U., Moshnyakov, M., Sariola, H., Sainio, K., Saarma, M., 1996. Localization of glial cell line-derived neurotrophic factor (GDNF) mRNA in embryonic rat by in situ hybridization. Eur. J. Neurosci. 8, 816–822.
Svingen, T., Spiller, C.M., Kashimada, K., Harley, V.R., Koopman, P., 2009. Identification of suitable normalizing genes for quantitative real-time RT-PCR analysis of gene expression in fetal mouse gonads. Sex Dev. 3, 194–204.
Tang, M.J., Worley, D., Sanicola, M., Dressler, G.R., 1998. The RET-glial cell-derived neurotrophic factor (GDNF) pathway stimulates migration and chemoattraction of epithelial cells. J. Cell Biol. 142, 1337–1345.
Wainwright, E.N., Svingen, T., Ng, E.T., Wicking, C., Koopman, P., 2014. Primary cilia function regulates the length of the embryonic trunk axis and urogenital field in mice. Dev. Biol. 395, 342–354.
Wilhelm, D., Hiramatsu, R., Mizusaki, H., Widjaja, L., Combes, A.N., Kanai, Y., Koopman, P., 2007. SOX9 regulates prostaglandin D synthase gene transcription in vivo to ensure testis development. J. Biol. Chem. 282, 10553–10560.
Yamaguchi, T.P., Bradley, A., McMahon, A.P., Jones, S., 1999. A Wnt5a pathway underlies outgrowth of multiple structures in the vertebrate embryo. Development 126, 1211–1223.
Young, H.M., Hearn, C.J., Farlie, P.G., Canty, A.J., Thomas, P.Q., Newgreen, D.F., 2001. GDNF is a chemoattractant for enteric neural cells. Dev. Biol. 229, 503–516.
Yun, K., Ajima, R., Sharma, N., Costantini, F., Mackem, S., Lewandoski, M., Yamaguchi, T.P., Perantoni, A.O., 2014. Non-canonical Wnt5a/Ror2 signaling regulates kidney morphogenesis by controlling intermediate mesoderm extension. Hum. Mol. Genet. 23, 6807–6814.